energies

Article

Current Sensor Fault Diagnosis and Tolerant Control for Nine-Phase PMSM Drives Based on Improved Axis Rotation

Xudong Zhang, Xiaoming Liu and Xiaoqin Zheng *

College of Electrical Engineering, Qingdao University, Qingdao 266071, China; zhangxd9636@163.com (X.Z.); lxm17863941238@163.com (X.L.)
* Correspondence: zhengxiaoqin@qdu.edu.cn; Tel.: +86-155-5320-0701

Abstract: Fault probability rises with an increase in the number of current sensors in multi-phase permanent synchronous motor (PMSM) drives. This paper proposes an improved axis rotation method for fault diagnosis and tolerant control to make the multi-phase PMSM drives against current sensor loss signal and gain faults. This method can effectively diagnose and distinguish faults without selecting a threshold value, and the degree of fault can be further estimated. The proposed method makes current sensor fault diagnosis and tolerant control become an integrated module. The validity and accuracy of the proposed method is verified by different fault diagnoses and tolerant control experiments of a 9 kw nine-phase PMSM drive.

Keywords: multi-phase motor drives; improved axis rotation; current sensor faults; fault tolerant control; faults degree estimation

check for updates

Citation: Zhang, X.; Liu, X.; Zheng, X. Current Sensor Fault Diagnosis and Tolerant Control for Nine-Phase PMSM Drives Based on Improved Axis Rotation. *Energies* **2022**, *15*, 4671. https://doi.org/10.3390/en15134671

Academic Editor: Silvio Simani

Received: 21 May 2022
Accepted: 24 June 2022
Published: 25 June 2022

1. Introduction

Multi-phase motor drives have strong application requirements in the high-reliability of multi-electric aircraft, ships and EVs due to their higher power density, lower torque ripple and superior fault tolerant capability [1–3]. However, the fault probability rises with an increase in the number of current sensors. In the operation process of multi-phase motor drives, over-voltage, over-current, aging and other harsh working environments may cause the current sensor output signal to be inaccurate [4,5]. The current sensor faults should be diagnosed and tolerated rapidly and effectively in applications with high-reliability requirements. The different current sensor faults will cause a different degree of distortion in the current feedback signals. It is necessary to accurately detect different types of faults in order to design corresponding fault tolerant control strategies. Therefore, it is significant to study the diagnosis and tolerant control of current sensor faults in multi-phase PMSM drives [6–8].

Current sensor faults have been effectively diagnosed and located in many existing literatures. The extended Kalman filter is suggested to detect the loss signal fault in [9]. The Kalman filter is merged with a system reconfiguration under the faults of the current sensor methods in [10] to diagnose the faults. A valid sliding mode observer (SMO) is adopted in [11] to diagnose the current sensor loss signal fault in PMSM sensorless control systems. The current error module is built based on the estimated signal error of the other health current sensors. Three reliable observers are suggested in [12] to observe the real-time state of three current sensors, therefore the loss signal fault can be located by the observers. Ref. [13] proposes an observer-based strategy relying on the adaptive threshold for fault location and tolerance. However, these observer models are easily affected by the motor parameters and operating environments. The signal-based methods need no complex calculation; only by signal processing can accurate sensor fault detection and tolerant control be obtained. Current signal analysis is combined with an SMO in [14], and the sensor loss signal fault is diagnosed through the space vector error-projection algorithm.

The phase and line voltage signal deviations strategy are presented in [15]. The loss signal faults can be diagnosed and isolated rapidly in both rectifier and inverter mode.

The above methods are only for current sensor loss signal fault detection and tolerant control. In addition to loss signal faults, the gain faults should also be detected and tolerated effectively. Fortunately, many efforts have been devoted to the research of loss signal and gain fault diagnosis. The state-observer-based algorithm shows its positive performance in current sensor loss signal and gain fault detection in [16,17]. In [18], the current estimations from an improved open-loop observer are adopted to obtain the fault detection and tolerant control. An algorithm programmed into the FPGA as a general controller is considered in [19]. For the three-phase PMSM systems, the fault diagnosis range in [19] is extended to loss signal and gain faults. The signal-based detection method with normalization in [20,21] has been widely used to achieve fault detection and tolerant control. The AC component of current analysis error is extracted by an improved filter in [22], and gain fault of the linear motor system is distinguished with other faults by the different frequency components. A modified algorithm combining a delay function and the current space vector is addressed in [23], which can detect and isolate loss signal and gain faults. Axis rotation is adopted in [24] for deciding the correct estimated value of the fault current sensor, and it shows good characteristics in the field of electric vehicle sensor fault detection and fault tolerance.

Considering different current sensor fault diagnosis and tolerant control for multi-phase PMSM drives, this paper proposes a method to diagnose both loss signal faults and gain faults based on improved axis rotation. Different from the existing literature, this signal-based method can accurately diagnose and effectively distinguish the loss signal and gain faults without additional hardware. By eliminating the selection of threshold value, the adaptability of this method to different operating conditions is also enhanced. Moreover, the degree of gain faults can be estimated quantitatively and it can be used to further tolerant control. Different types of current sensor faults are matched with corresponding fault tolerant control strategies. The method makes current sensor fault diagnosis and tolerant control become an integrated module. This article is structured as follows: The topology of nine-phase PMSM drives is introduced in Section 2. The influence on currents of current sensor loss signal faults and gain faults are analyzed in Section 3. The proposed diagnosis and tolerant control method are illustrated in Sections 4 and 5, respectively. The corresponding experiments of a 9 kw nine-phase PMSM are carried out to verify the effectiveness and accuracy of the proposed method in Section 6. A conclusion is drawn in Section 7.

2. Influence of Current Sensor Faults on Drive Systems

The nine-phase PMSM in this article is composed of three sets of three-phase open-end windings which are spatially shifted $\pi/9$ degrees. Each phase is equipped with an independent current sensor. An H-bridge inverter circuit drives nine-phase effectively with more control, reliability, and independence. Figure 1a shows the nine-phase PMSM windings structure, and Figure 1b shows the nine-phase H-bridge drive topology.

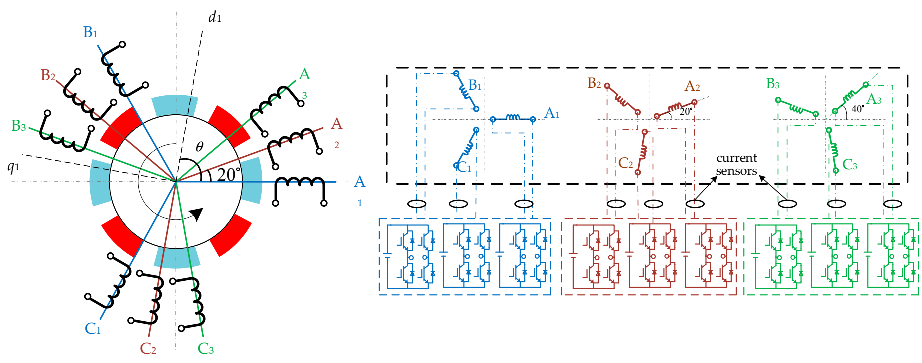

Figure 1. (**a**) Winding structure of nine-phase PMSM; (**b**) H-bridge drive topology.

The probability of faults increases with the number of current sensors required for the nine-phase PMSM drives. The fault diagnosis and tolerant control of nine-phase PMSM drives are shown in Figure 2.

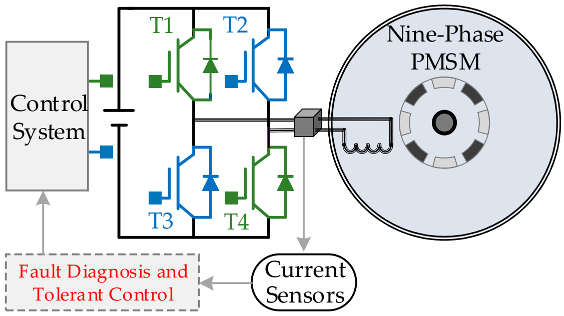

Figure 2. Diagram of diagnosis and tolerant control of nine-phase PMSM drives.

3. Influence of Current Sensor Faults on Motor Drives

Based on the frequency of faults and the degree of negative impact on the motor drives, the typical current sensor faults distinguished by output characteristics can be classified as gain fault and loss signal fault. Taking phase-A_1 current sensor faults as an example, the measured phase currents of each sensor can be expressed as:

$$\begin{aligned} & i_{\mathrm{A1}} = \lambda i^*{}_{\mathrm{A1}} = \lambda I_{\mathrm{am}} \cos(\omega t + \theta_{\mathrm{ori}}) \\ & i_{\mathrm{A2}} = i^*{}_{\mathrm{A2}} \\ & \vdots \\ & i_{\mathrm{C3}} = i^*{}_{\mathrm{C3}} \end{aligned} \tag{1}$$

where, $i^*{}_{\mathrm{A1}}$, $i^*{}_{\mathrm{A2}} \ldots i^*{}_{\mathrm{C3}}$ are the real phase currents, i_{A1}, $i_{\mathrm{A2}} \ldots i_{\mathrm{C3}}$ are the measured values by nine-phase current sensors, λ is the gain coefficient of fault current sensor, I_{am} is the phase current amplitude, θ_{ori} is the initial phase angle and ω is the electrical angular frequency respectively.

In normal conditions, $\lambda = 1$; when loss signal faults occur, $\lambda = 0$; when gain faults occur, $\lambda > 1$. The expression of i_{d1} and i_{q1} in the d-q coordinate is in Equation (2).

$$\begin{bmatrix} i_{d1} \\ i_{q1} \end{bmatrix} = \frac{2}{9} * \begin{bmatrix} \cos\theta_e & \ldots & \cos(\theta_e - 14\pi/9) \\ -\sin\theta_e & \ldots & -\sin(\theta_e - 14\pi/9) \end{bmatrix} \begin{bmatrix} i_{\mathrm{A1}} \\ \cdots \\ i_{\mathrm{C3}} \end{bmatrix} \tag{2}$$

Assuming that the fault of the phase-A_1 current sensor in the multi-phase motor drives has little effect on the normal phase current amplitude, Equation (1) is substituted into Equation (2), then the measured value of i_{q1_m} can be expressed.

$$\begin{aligned} i_{q1\_m} &= i_{q1} - \tfrac{2}{9} * (\lambda - 1) * i_{\mathrm{A1}} * \sin\theta_e - \tfrac{2}{9} * \sin\theta_e \\ &= i_{q1} - \underbrace{\frac{(\lambda - 1) I_{am} \sin(2\omega t + \theta_{ori})}{9}}_{\mathrm{AC}} + \underbrace{\frac{(\lambda - 1) I_{am} \sin(\theta_{ori})}{9}}_{\mathrm{DC}} \end{aligned} \tag{3}$$

1. In normal conditions, $\lambda = 1$, DC component is zero, so i_{q1} is equal to i_{q1_m} with no bias.
2. When loss signal faults occur, the real phase currents are not measured by current sensors. The AC component are zero-mean pulsations; DC component is a bias less than zero due to $\lambda = 0$.
3. When gain faults occur, the AC component is still zero-mean pulsations, but the DC component is a bias greater than zero due to $\lambda > 1$.

Therefore, the i_{q1_m} impacted by the DC component can be used as the characteristic quantity to distinguish normal conditions, loss signal faults and gain faults. In addition to the fault type, the location of the fault point is also essential, so it is necessary to further propose a perfect diagnosis strategy combined with i_{q1_m}.

4. Diagnosis for Current Sensors Faults

4.1. Improved Axis Rotation

From the transformation matrix of the semi-symmetric nine-phase PMSM natural coordinate system to the synchronous stationary coordinate system (Clark), it can be seen that in the standard transformation shown in Figure 3, A_1-axis and α_1-axis are in the same direction. The component of phase current i_{A1} on β_1-axis is zero and the component on α_1-axis is 100% i_{A1}.

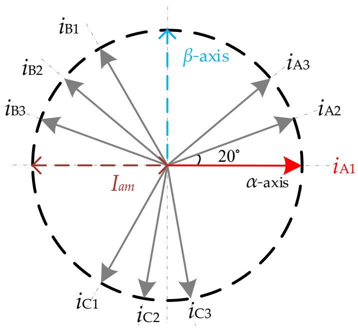

Figure 3. The standard Clark transformation.

Therefore, from the $i_{\alpha 1}$ and $i_{\beta 1}$ in Equation (4), only the current sensor fault of phase-A_1 has the least influence on $i_{\beta 1}$ and the largest influence on $i_{\alpha 1}$ among all nine phases.

$$\begin{bmatrix} i_{\alpha 1\_1} \\ i_{\beta 1\_1} \end{bmatrix} = \frac{2}{9} * \begin{bmatrix} 1 & \cos\frac{\pi}{9} & \dots & \cos\frac{14\pi}{9} \\ 0 & \sin\frac{\pi}{9} & \dots & \sin\frac{14\pi}{9} \end{bmatrix} \begin{bmatrix} i_{A1} \\ i_{A2} \\ \dots \\ i_{C3} \end{bmatrix} \tag{4}$$

where, $i_{\alpha 1\_1}$ and $i_{\beta 1\_1}$ are fundamental wave currents of α and β when phase-A_1 is used as reference axis.

In general, regarding the other phases, when different phase-N is selected as the reference axis, the Clark matrix will shift different angles θ_N, and current sensor faults of reference phase-N has the least influence on the corresponding $i_{\beta 1\_N}$, and the largest influence on $i_{\alpha 1\_N}$. The general formula of $i_{\alpha 1\_N}$ and $i_{\beta 1\_N}$ can be obtained in Equation (5).

$$\begin{bmatrix} i_{\alpha 1-N} \\ i_{\beta 1-N} \end{bmatrix} = \begin{bmatrix} \cos(0-\theta_N) & \cos(\frac{\pi}{9}-\theta_N) & \dots & \cos(\frac{14\pi}{9}-\theta_N) \\ \sin(0-\theta_N) & \sin(\frac{\pi}{9}-\theta_N) & \dots & \sin(\frac{14\pi}{9}-\theta_N) \end{bmatrix} \begin{bmatrix} i_{A1} \\ i_{A2} \\ \dots \\ i_{C3} \end{bmatrix} \tag{5}$$

where, the θ_N of stator windings of semi-symmetric nine-phase motor system can be expressed as:

$$\theta_N \in \begin{bmatrix} 0 & \frac{2\pi}{9} & \frac{4\pi}{9} & \frac{6\pi}{9} & \frac{7\pi}{9} & \frac{8\pi}{9} & \frac{12\pi}{9} & \frac{13\pi}{9} & \frac{14\pi}{9} \end{bmatrix} \tag{6}$$

When different phases are selected as reference axes, the expressions of $i_{\alpha 1\_N}$ and $i_{\beta 1\_N}$ can be obtained in Equation (7).

$$\begin{aligned}
\begin{bmatrix} i_{\alpha 1-1} \\ i_{\alpha 1-2} \\ \cdots \\ i_{\alpha 1-9} \end{bmatrix} &= \begin{bmatrix} i_{A1} * 1 + i_{A2} * \cos \pi/9 + \ldots + i_{C3} * \cos 14\pi/9 \\ i_{A1} * \cos \pi/9 + i_{A2} * 1 + \ldots + i_{C3} * \cos 13\pi/9 \\ \cdots \\ i_{A1} * \cos 14\pi/9 + i_{A2} * \cos 13\pi/9 + \ldots + i_{C3} * 1 \end{bmatrix} \\
\begin{bmatrix} i_{\beta 1-1} \\ i_{\beta 1-2} \\ \cdots \\ i_{\beta 1-9} \end{bmatrix} &= \begin{bmatrix} i_{A1} * 0 + i_{A2} * \sin \pi/9 + \ldots + i_{C3} * \sin 14\pi/9 \\ -i_{A1} * \sin \pi/9 + i_{A2} * 0 + \ldots + i_{C3} * \sin 13\pi/9 \\ \cdots \\ -i_{A1} * \sin 14\pi/9 - i_{A2} * \sin 13\pi/9 - \ldots - i_{C3} * 0 \end{bmatrix}
\end{aligned} \tag{7}$$

Therefore, the above formula shows that the $i_{\alpha 1\_1}$ changes the most in all $i_{\alpha 1\_N}$ when loss signal fault (i_{A1} = 0) occurs in phase-A_1, which is equivalent to the $i_{\alpha 1\_1}$ losing 100% of i_{A1} and $i_{\alpha 1\_1}$ has the lowest mean value in all $i_{\alpha 1\_N}$. Also, $i_{\beta 1\_1}$ has the smallest change in all $i_{\beta 1\_N}$, and the other eight $i_{\beta 1\_N}$ have lost sinπ/9, sin2π/9 . . . sin14π/9 times of i_{A1}, respectively.

1. In normal conditions, nine $i_{\alpha 1\_N}$ have the same mean value, and so do nine $i_{\beta 1\_N}$.
2. When loss signal fault (i_{A1} = 0) occurs in phase-A_1, the above formula shows that the $i_{\alpha 1\_1}$ changes the most in all $i_{\alpha 1\_N}$, which is the equivalent to the $i_{\alpha 1\_1}$ losing 100% of i_{A1}, and $i_{\alpha 1\_1}$ has the lowest mean value in all $i_{\alpha 1\_N}$. Also, $i_{\beta 1\_1}$ has the smallest change in all $i_{\beta 1\_N}$, and the other eight $i_{\beta 1\_N}$ have lost sinπ/9, sin2π/9...sin14π/9 times of $i_{\alpha 1\_1}$, respectively.
3. When gain fault ($i_{A1} = \lambda i^{*}{}_{A1}$) occurs in phase-$A_1$, $i_{\alpha 1\_1}$ has the largest change in all $i_{\alpha 1\_N}$, equivalent to $i_{\alpha 1\_1}$ increased by 100% "$(\lambda - 1) i_{A1}$", which has the largest mean of all $i_{\alpha 1\_N}$. Additionally, $i_{\beta 1\_1}$ has the smallest change in all $i_{\beta 1\_N}$. The other phases have gained sinπ/9, sin2π/9 . . . sin14π/9 times of $(\lambda - 1) i_{A1}$, respectively. $i_{\beta 1\_1}$ has the smallest mean in all $i_{\beta 1\_N}$.

Therefore, if the mean value difference of each $i_{\alpha 1\_N}$ and $i_{\beta 1\_N}$ is selected for comparison, the difference corresponding to the fault phase is the largest, which can be used as the characteristic quantity for locating the fault phase. Taking phase-A_1 faults as an example, in combination with Equation (7), the reference vectors of $i_{\alpha 1\_N}$ and $i_{\beta 1\_N}$ in each axis rotation coordinate system are shown in Figure 4.

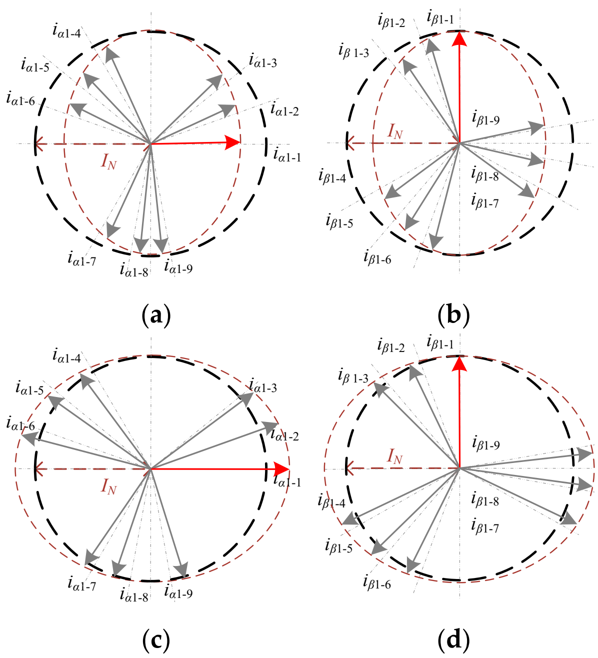

Figure 4. (**a**) $i_{\alpha 1\_N}$ in loss signal fault; (**b**) $i_{\beta 1\_N}$ in loss signal fault; (**c**) $i_{\alpha 1\_N}$ in gain fault; (**d**) $i_{\beta 1\_N}$ in gain fault.

The proposed method is based on the principle of axis rotation; $i_{\alpha 1\_N}$ and $i_{\beta 1\_N}$ always change in reverse direction after a fault, so the diagnosis variables can be designed by combining them.

4.2. Diagnosis Strategy

Based on the above derivation, this paper proposes a fault diagnosis method of current sensor based on improved axis rotation. The fault diagnosis of a multi-phase motor can be realized by analyzing the sampled current information of the system. Its diagnosis principle is shown in Figure 5.

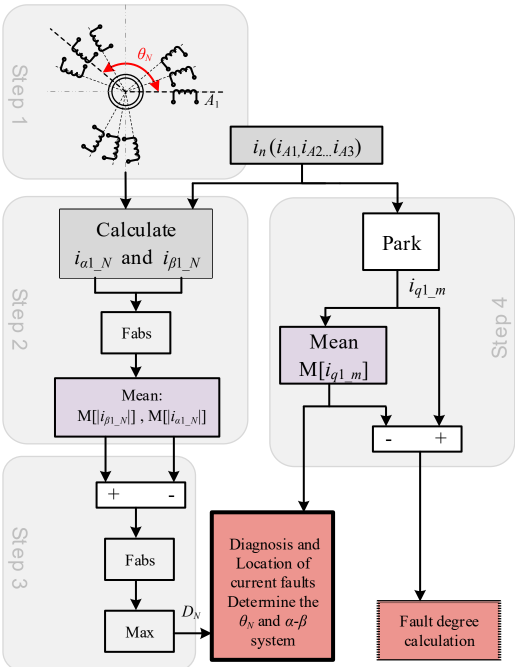

Figure 5. Block diagram of proposed method.

Step 1: The rotation angle θ_N of different phases in the multi-phase motor should be determined, and the expressions of $i_{\alpha 1\_N}$ and $i_{\beta 1\_N}$ with different reference phases as α_1-axis should be established according to θ_N. Nine-phase motors correspond to 2 × 9 expressions.

Step 2: $i_{\alpha 1\_N}$ and $i_{\beta 1\_N}$ are respectively defined as $i_{\alpha 1\_N} = I_{am1}\cos(\omega t - \theta_N)$, $i_{\beta 1\_N} = I_{am2}\sin(\omega t - \theta_N)$, where I_{am1} and I_{am2} are the current amplitude. M[$|i_{\alpha 1\_N}|$] and M[$|i_{\beta 1\_N}|$] are respectively obtained by the absolute-mean processor in Equation (8).

$$\begin{aligned} \mathrm{M}[|i_{\alpha 1\_N}|] &= \frac{\omega}{2\pi}\int_0^{\frac{2\pi}{\omega}} |I_{\mathrm{am1}}\cos(\omega t - \theta_N)|\mathrm{dt} = \frac{2}{\pi}I_{\mathrm{am1}} \\ \mathrm{M}[|i_{\beta 1\_N}|] &= \frac{\omega}{2\pi}\int_0^{\frac{2\pi}{\omega}} |I_{\mathrm{am2}}\cos(\omega t - \theta_N)|\mathrm{dt} = \frac{2}{\pi}I_{\mathrm{am2}} \end{aligned} \quad (8)$$

When current sensor fault occurs, the absolute-mean difference between $i_{\alpha 1\_N}$ and $i_{\beta 1\_N}$ is the largest in the axis rotation coordinate system corresponding to the fault phase. Therefore, the difference of M[$|i_{\alpha 1\_N}|$] and M[$|i_{\beta 1\_N}|$] can distinguish between fault and health phases.

Step 3: The fault phase of the current sensor can be located by diagnosis variables "D_N = Max($|$M[$|i_{\beta 1_N}|$]-M[$|i_{\alpha 1_N}|$]$|$)" after screened by the maximum calculator. The proposed method eliminates the selection of threshold value, and the phase with the strictest maximum in the all D_N corresponding to the nine-phase currents is the fault phase, which greatly reduces the probability of misdiagnosis.

Step 4: The above algorithm realizes the location of the fault current sensor. However, to distinguish between gain faults and loss signal faults, the q_1-axis current i_{q1_m} is used.

After processed by a mean processor and combined with Equation (3), the expression of $M[i_{q1\_m}]$ can be obtained:

$$\begin{aligned} M[i_{q1\_m}] &= \frac{\omega}{2\pi}\int_0^{\frac{2\pi}{\omega}} i_{q1\_m}dt \\ &= M[i_{q1}] - \underbrace{M[\frac{(\lambda-1)I_{am}\sin(2\omega t+\theta_{ori})}{9}]}_{M[AC]} + \underbrace{M[\frac{(\lambda-1)I_{am}\sin(\theta_{ori})}{9}]}_{M[DC]} \\ &= i_{q1} + \frac{(\lambda-1)I_{am}\sin(\theta_{ori})}{9} \end{aligned} \tag{9}$$

1. In normal conditions, λ = 1, DC = 0, $M[i_{q1\_m}] = i_{q1\_m}$. There was no change in i_{q1_m}.
2. When loss signal fault occurs, λ = 0, M[AC] is a zero-mean value. So, $M[i_{q1\_m}] = i_{q1}\text{-}I_{am}\sin(\theta_{ori})/9$.
3. When gain faults occurs, $\lambda > 1$, M[AC] is still a zero-mean value, but $M[i_{q1\_m}] = i_{q1} + (\lambda-1)I_{am}\sin(\theta_{ori})/9$.

Therefore, $M[i_{q1\_m}]$ will be biased with different properties when the current sensor fault occurs, and the bias caused by loss signal faults and gain faults must be opposite. Therefore, the next key is to determine the DC component "$I_{am}\sin(\theta_{ori})/9$".

Since i_{q1_m} can be considered to be derived from the nine-phase current through Park transformation in Equation (5), $M[i_{q1\_m}]$ is equivalent to the mean action of the nine-phase currents, that is, $M[i_{q1\_m}] = M[\cos\theta_e \times i_{A1}] + \ldots + M[\cos(\theta_e - 14\pi/9) \times i_{C3}]$. Therefore, $M[i_{q1\_m}]$ will become "8/9" of its original value after a phase current sensor fault. The expression of $M[i_{q1\_m}]$ after faults can be obtained:

1. In normal conditions, i_{q1_m} has no DC component, $i_{q1\_m} = i_{q1}$.
2. When loss signal fault occurs, the DC component causes i_{q1_m} to be 1/9 less than the i_{q1_m} in normal conditions, that is, $I_{am}\sin(\theta_{ori})/9 = i_{q1}/9$.

$$M[i_{q1\_m}] = i_{q1} - \frac{I_{am}\sin(\theta_{ori})}{9} = \frac{8}{9}i_{q1} < i_{q1} \tag{10}$$

3. When gain fault occurs, the DC component causes i_{q1_m} more $(\lambda-1)I_{am}\sin(\theta_{ori})/9$ than i_{q1_m} in normal operation.

$$M[i_{q1\_m}] = i_{q1} + \frac{(\lambda-1)I_{am}\sin(\theta_{ori})}{9} = i_{q1} + \frac{(\lambda-1)i_{q1}}{9} > i_{q1} \tag{11}$$

Therefore, the loss signal faults and gain faults can be distinguished by comparing the bias direction of $M[i_{q1\_m}]$ after the faults occur.

Different from the loss signal faults, if the gain coefficient λ can be obtained when the gain fault occurs, the fault tolerant operation can be realized only by adjusting the factor of current sampling. From Equation (11), it can be concluded that the gain fault causes the fault i_{q1_m} to be $(\lambda-1)i_{q1}/9$ larger than normal i_{q1_m}. So λ can be obtained by Equation (12).

$$\lambda = \frac{9(M[i_{q1\_m}] - i_{q1})}{i_{q1}} + 1 \tag{12}$$

Combining with the diagnosis variables D_N and $M[i_{q1\_m}]$, the current sensor gain and loss signal faults can be distinguished and located, the gain coefficient λ of fault degree is obtained, which is prepared for fault tolerant in the next stage. The diagnosis method proposed in this paper is shown in Figure 6.

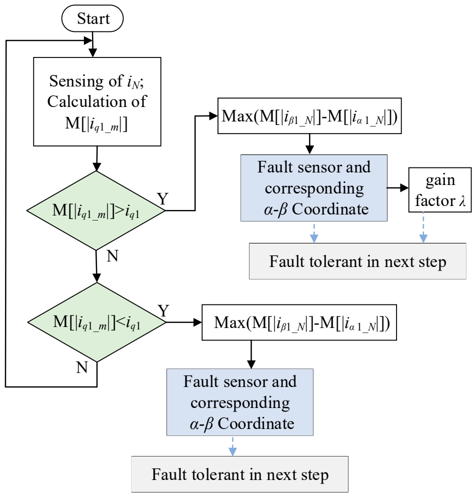

Figure 6. Flowchart of proposed method.

5. Tolerant Control of Current Sensors Faults

According to Section 2, i_{q1_m} will produce different forms of pulsation and bias when the current sensor faults occur, thus affecting the stable operation of the control system. Therefore, the key to fault tolerant of current sensor depends on the correct estimation of feedback current i^*_{d1} and i^*_{q1}. i_{d1} and i_{q1} are derived from $i_{\beta1\_N}$ and $i_{\alpha1\_N}$, so as long as the correct $i^*_{\beta1\_N}$ and $i^*_{\alpha1\_N}$ is estimated by the appropriate algorithm, the fault tolerant operation of current sensors can be realized.

The fault diagnosis in Section 3 can locate the corresponding phase of the fault current sensor, and then determine the corresponding θ_{A1} of axis rotation system. Taking phase-A_1 as a fault example, in its corresponding rotation system, the phase current $i_{\beta1\_1}$ remains unchanged before and after the fault, so $i_{\beta1\_1}$ can be used as the β_1-axis fault tolerant current $i^*_{\beta1}$ after the fault. The calculation of α_1-axis fault tolerant current $i^*_{\alpha1}$ is discussed as follows. According to Equation (10), the $M[i_{q1\_m}]$ after loss signal fault and its value in normal conditions meet Equation (13):

$$i_{q1} = \frac{9}{8}M[i_{q1\_m}] \tag{13}$$

So α_1-axis fault tolerant current $i^*_{\alpha1}$ can be obtained by the anti-Park matrix in Equation (13).

$$i^*_{\alpha1} = \begin{bmatrix} \cos(\theta_e - \theta_{A1}) & -\sin(\theta_e - \theta_{A1}) \end{bmatrix} \begin{bmatrix} \frac{9}{8}M[i_{q1\_m}] \\ i^*_{d1} \end{bmatrix} \tag{14}$$

Among them, the rotation angle θ_{A1} of the transformation matrix in Equation (14) should be selected in accordance with the θ_{A1} determined by the fault diagnosis module.

After $i^*_{\alpha1}$ and $i^*_{\beta1}$ are determined, the feedback current i^*_{d1} and i^*_{q1} can be obtained from the rotation matrix corresponding to θ_{A1}.

$$\begin{bmatrix} i^*_{d1} \\ i^*_{q1} \end{bmatrix} = \begin{bmatrix} \cos(\theta_e - \theta_{A1}) & \sin(\theta_e - \theta_{A1}) \\ -\sin(\theta_e - \theta_{A1}) & \cos(\theta_e - \theta_{A1}) \end{bmatrix} \begin{bmatrix} i^*_{\alpha1} \\ i^*_{\beta1} \end{bmatrix} \tag{15}$$

i^*_{d1} and i^*_{q1} are incorporated into the control system as fault tolerant feedback to realize fault tolerant operation of current sensor fault. Thus, $i^*_{\alpha1}$, $i^*_{\beta1}$, i^*_{d1} and i^*_{q1} are obtained by rotation transformation with the same angle θ_{A1}. The θ_{A1} corresponding to the fault can be determined only by the fault detection module, that is, fault diagnosis and fault tolerant operate in the same rotation transformation system, realizing the integration of diagnosis and fault tolerant. It is worth noting that the combination of fault diagnosis and fault-tolerant control module needs to consider the correspondence of θ_N. As a bridge connecting diagnosis and tolerance, the selection of θ_N determines the accuracy of fault tolerance current i^*_{q1}. Moreover, for gain faults, fault-tolerant control can be realized directly and accurately only by compensating a calculated gain coefficient λ (Equation (12)) for the fault phase current.

The proposed method used stator currents to diagnosis current sensor faults and obtained tolerant control by estimating and switching the i_{q1}. Therefore, is strongly adaptable to a different controller. Additionally, the discussion and verification of the proposed method in this paper are operated under a vector control system (Figure 7).

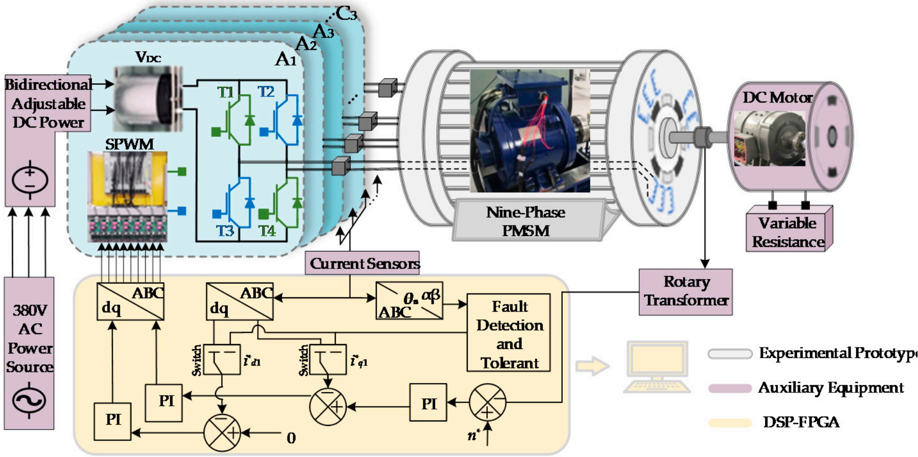

Figure 7. Control system of a nine-phase PMSM motor.

6. Experimental Verification

6.1. Experimental Setup

In order to verify the validity of the fault diagnosis and fault tolerant method proposed in this paper, an experimental platform of nine-phase PMSM was built. The platform consists of a DC power, a controller, a 9 kw nine-phase PMSM, a DC motor, a speed-torque measuring instrument, and a voltage source inverter (VSI). The 9 kw nine-phase PMSM is powered by VSI; H-bridge inverter circuits drive each phase respectively, and the load shaft is connected with a DC generator. The block diagram of the motor control principle is shown Figure 7. The parameters of nine-phase PMSM are shown in Table 1.

Table 1. Nine-phase PMSM parameters.

Parameters	Value
Power	9 kw
Voltage	234 V
Current	4.6 A
Speed	900 rpm
Torque	95.5 Nm
d-axis inductance	41.2 mH
q-axis inductance	41.2 mH
Armature resistance	2.47 Ω
Magnet flux linkage	0.8524 Wb
pole-pairs	4
Rotational inertia/kg·m^2	0.03128

6.2. Loss Signal Fault Diagnosis

Some literature on axis rotation uses the difference between $i_{\alpha 1\_1}$ and $i^*_{\alpha 1\_1}$ as diagnosis variables [24]. Thresholds are introduced to distinguish normal conditions from current sensor faults. Because this threshold is so similar in gain and loss signal faults (Figure 8), the algorithm presented in [24] cannot distinguish them effectively.

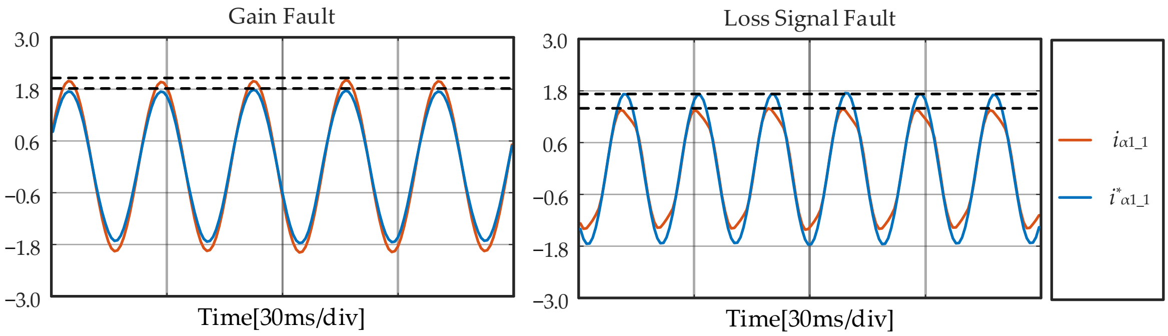

Figure 8. $i_{\alpha1\_1}$ and $i^*_{\alpha1\_1}$ in different faults.

In this paper, the mean value difference of each $i_{\alpha1\_N}$ and $i_{\beta1\_N}$ is selected for comparison, the "D_N = Max(|M[|$i_{\beta1\_N}$|] − M[|$i_{\alpha1\_N}$|])" corresponding to the fault phase is the largest, which can be used to locate the fault without the selection of a threshold.

First, the motor operates stably with 25 Nm load. Then, the output of the phase-A_1 current sensor is set to zero through simulation in DSP. The corresponding $i^*_{\alpha1\_N}$ and $i^*_{\beta1\_N}$ are shown in Figure 9.

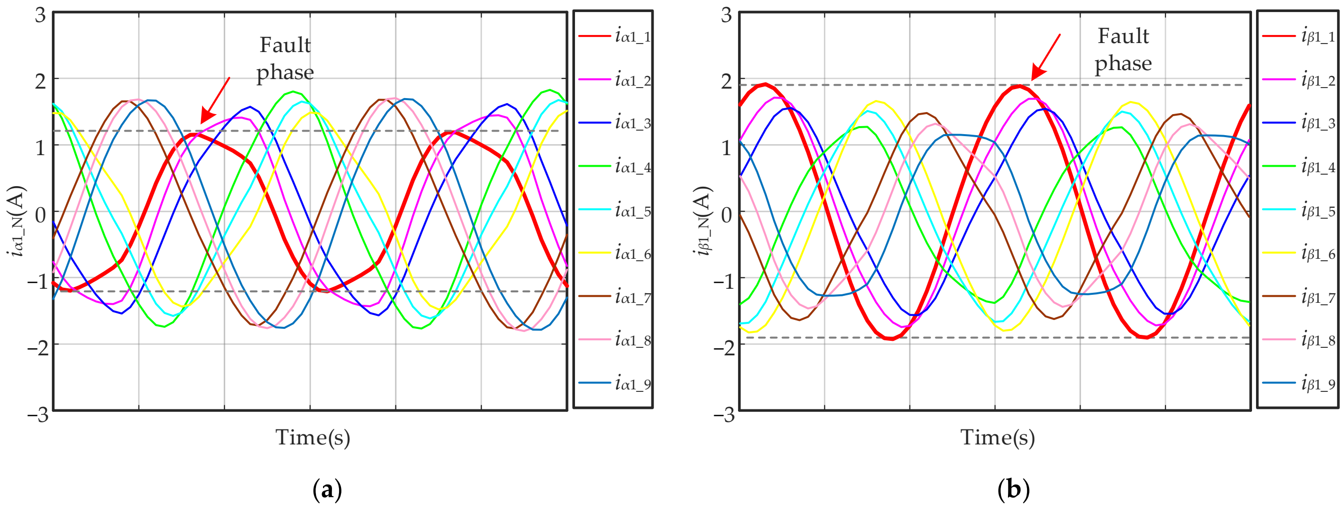

Figure 9. (**a**) $i_{\alpha1\_N}$ in loss signal fault; (**b**) $i_{\beta1\_N}$ in loss signal fault.

When i_{A1} = 0, the loss signal fault occurs in phase-A_1. According to the Equation (7), among the nine $i_{\alpha1\_N}$ and $i_{\beta1\_N}$ obtained by the axis rotation system, $i_{\alpha1\_1}$ is most affected and $i_{\beta1\_1}$ keeps the amplitude almost constant. Thus, it can be seen in the Figure 8 that $i_{\alpha1\_1}$ becomes the current with the lowest amplitude, and conversely, $i_{\beta1\_1}$ becomes the one with the highest amplitude.

Figure 10 shows the M[|$i_{\alpha1\_N}$|] and M[|$i_{\beta1\_N}$|] calculated by absolute-mean processors. Due to the linear relationship between amplitude and absolute-mean in Equation (8), the value of M[|$i_{\alpha1\_1}$|] is the smallest of the nine M[|$i_{\alpha1\_N}$|]. Similarly, M[|$i_{\beta1\_1}$|] is the largest one of the nine M[|$i_{\beta1\_N}$|].

Figure 11 shows the diagnosis variables D_N and M[i_{q1_m}]. In normal conditions, each D_N are almost equal and approximately zero. When a current sensor fault occurs, the difference between M[|$i_{\alpha1\_N}$|] and M[|$i_{\beta1\_N}$|] of the fault phase is strictly maximum in Figure 10. Therefore, D_1 is the max value of nine D_N, so the fault phase can be located. Moreover, i_{q1_m} has a negative DC bias "$-I_{am}\sin(\theta_{ori})/9$", a zero-mean pulse. Thus, M[i_{q1_m}] in a loss signal fault is less than it is in normal conditions, so the loss signal fault of phase-A_1 current sensor can be diagnosed.

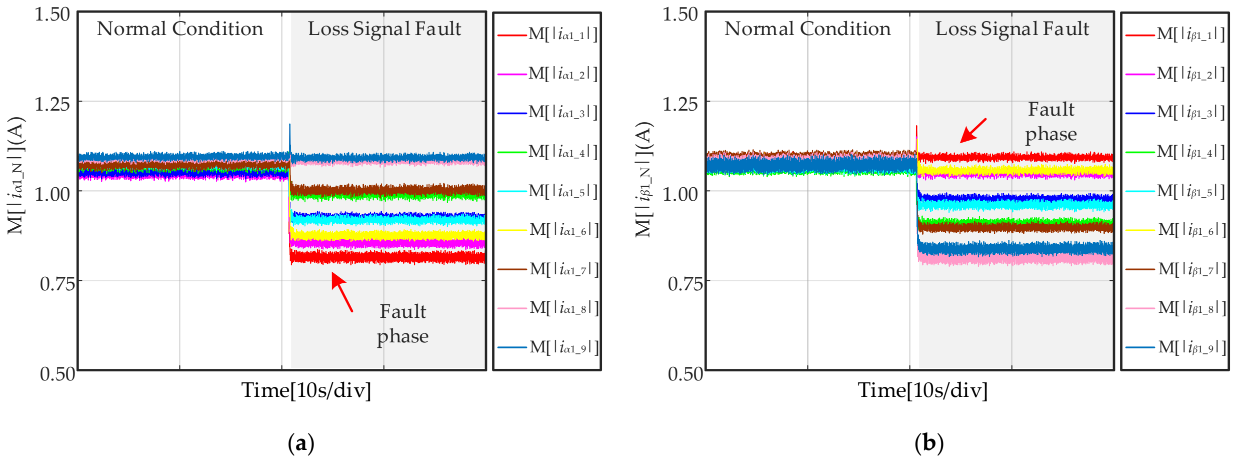

Figure 10. (**a**) M[| $i_{\alpha 1\_N}$ |] in loss signal fault; (**b**) M[| $i_{\beta 1\_N}$ |] in loss signal fault.

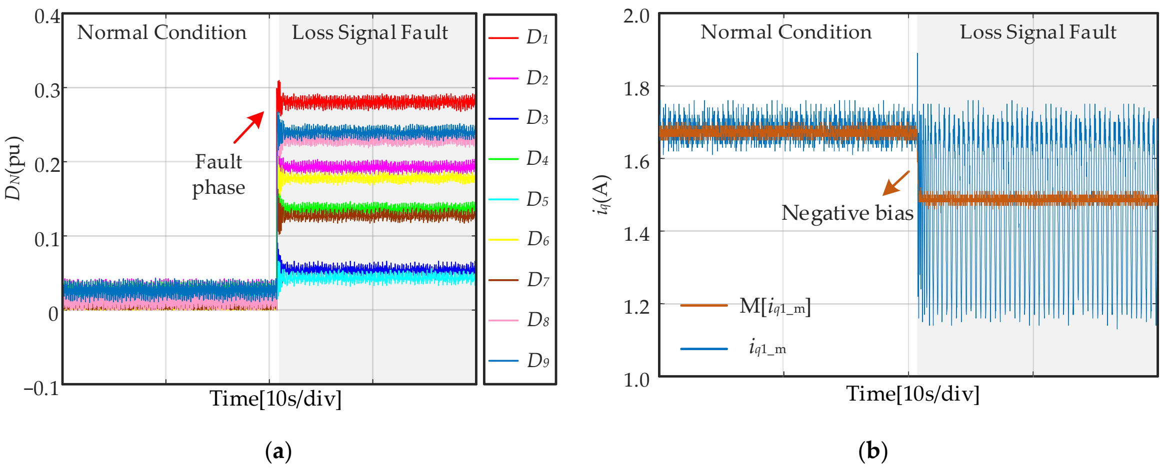

Figure 11. (**a**) D_N in loss signal fault; (**b**) M[i_{q1_m}] and i_{q1_N} in loss signal fault.

6.3. Gain Fault Diagnosis

This fault diagnosis experiment is to verify the validity of the proposed method for current sensor gain fault. When a 2.5 times gain fault of phase-A_1 current sensor is set through simulation in DSP. The corresponding $i^*{}_{\alpha 1\_N}$ and $i^*{}_{\beta 1\_N}$ are shown in Figure 12.

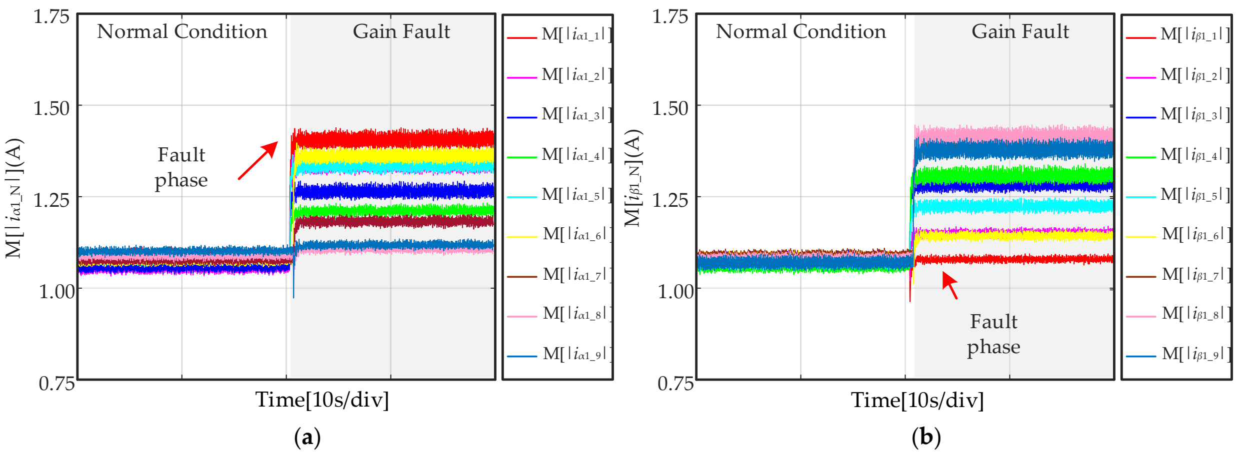

Figure 12. (**a**) M[| $i_{\alpha 1\_N}$ |] in gain fault; (**b**) M[| $i_{\beta 1\_N}$ |] in gain fault.

When the loss signal fault occurs in phase-A_1 ($i_{A1} = 2.5i^*_{A1}$), $i_{\alpha 1\_1}$ is most affected while $i_{\beta 1\_1}$ keeps the constant amplitude. According to Equation (7), $i_{\alpha 1\_1}$ becomes the current with the largest amplitude and $i_{\beta 1\_1}$ becomes the one with the smallest amplitude. The $M[|i_{\alpha 1\_N}|]$ and $M[|i_{\beta 1\_N}|]$ calculated by absolute-mean processors are shown in Figure 12. Therefore, the value of $M[|i_{\alpha 1\_1}|]$ is the largest of the nine $M[|i_{\alpha 1\_N}|]$, and $M[|i_{\beta 1\_1}|]$ is the smallest one of the nine $M[|i_{\beta 1\_N}|]$.

Figure 13 shows the diagnosis variables D_N and $M[i_{q1\_m}]$. Each D_N are approximately zero in normal conditions. When the fault occurs, the difference between $M[|i_{\alpha 1\_N}|]$ and $M[|i_{\beta 1\_N}|]$ of the fault phase is strictly maximum in Figure 13. Therefore, D_1 is also the max value of D_N, so the fault phase-A_1 can be located. Moreover, i_{q1_m} has a distinct positive DC bias "$1.5I_{am}\sin(\theta_{ori})/9$" and a zero-mean pulse. Thus, $M[i_{q1\_m}]$ in loss signal fault is greater than it is in normal conditions, which can be used to further diagnose tolerant control. So, the loss signal fault of phase-A_1 current sensor can be diagnosed.

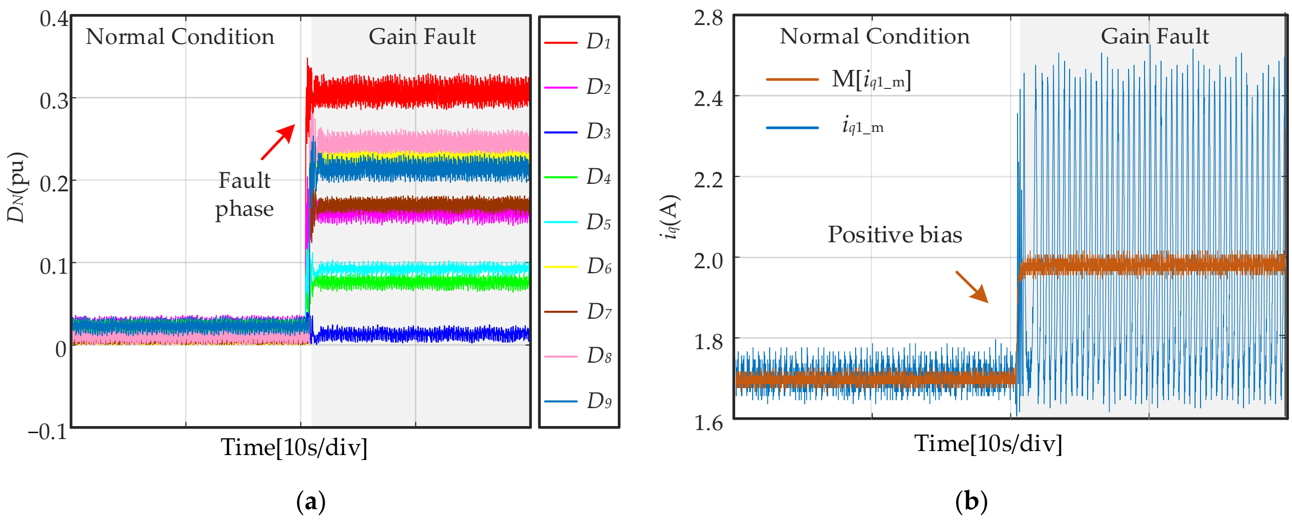

Figure 13. (**a**) D_N in gain fault; (**b**) $M[i_{q1\_m}]$ and i_{q1_N} in gain fault.

The threshold selection is eliminated in the whole diagnosis process, and the loss signal faults can be located by selecting the phase with the maximum value of the diagnosis variables D_N. $M[i_{q1\_m}]$ has an obvious negative bias feature, which makes the distinction between loss signal and gain faults more accurate.

6.4. Loss Signal Fault Tolerant

In order to verify the effectiveness of the proposed fault tolerant method, the loss signal fault-tolerant control experiment is shown as follows: $i_{\alpha 1\_1}$ and $i_{\beta 1\_1}$ are the actual currents, $i^*_{\alpha 1\_1}$ and $i^*_{\beta 1\_1}$ are the fault tolerant currents. Since $i_{\beta 1\_1}$ remains almost constant when fault occurs, $i_{\beta 1\_1}$ can be directly referred to as $i^*_{\beta 1\_1}$. And the conversion between i_{q1_m} and fault tolerant current i^*_{q1} is realized by the switch designed in DSP.

In Figure 14, $i_{\alpha 1\_1}$ and $i_{\beta 1\_1}$ ($i^*_{\beta 1\_1}$) have similar amplitude in normal conditions. However, due to the existence of a correction factor of 9/8 in Equation (12), the amplitude of the fault tolerant current $i^*_{\alpha 1\_1}$ is slightly higher than $i_{\alpha 1\_1}$ and $i^*_{\beta 1\_1}$. When the loss signal fault occurs in A_1, $i_{\alpha 1\_1}$ is most affected and $i^*_{\beta 1\_1}$ keeps almost constant but the tolerant current $i^*_{\alpha 1\_1}$ has the same amplitude as $i_{\alpha 1\_1}$ in normal condition. Before and after the fault-tolerant control, $i^*_{\alpha 1\_1}$ can maintain a stable correct amplitude, so that it can be connected to the system together with $i^*_{\beta 1\_1}$ as the fault tolerant current.

Figure 15 shows that i_{q1_m} produces a large pulse due to the DC bias and AC pulsation when faults occur. At this time, the current i_{Q1} connected to the feedback system is still i_{q1_m}. Then, the switch is given a fault tolerant signal and it selects i^*_{q1} to be transferred to the output. Therefore, the feedback current i_{Q1} is restored to i_{q1_m} in normal condition, and fault-tolerant control is realized.

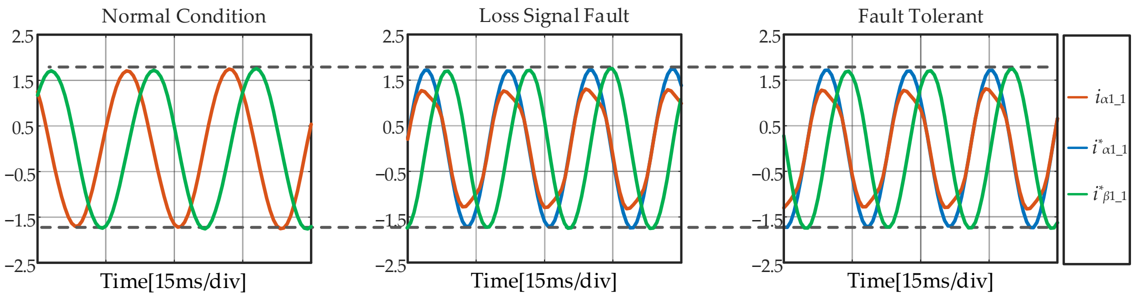

Figure 14. $i_{\alpha 1\_1}$, $i^*_{\alpha 1\_1}$ and $i^*_{\beta 1\_1}$ in different conditions.

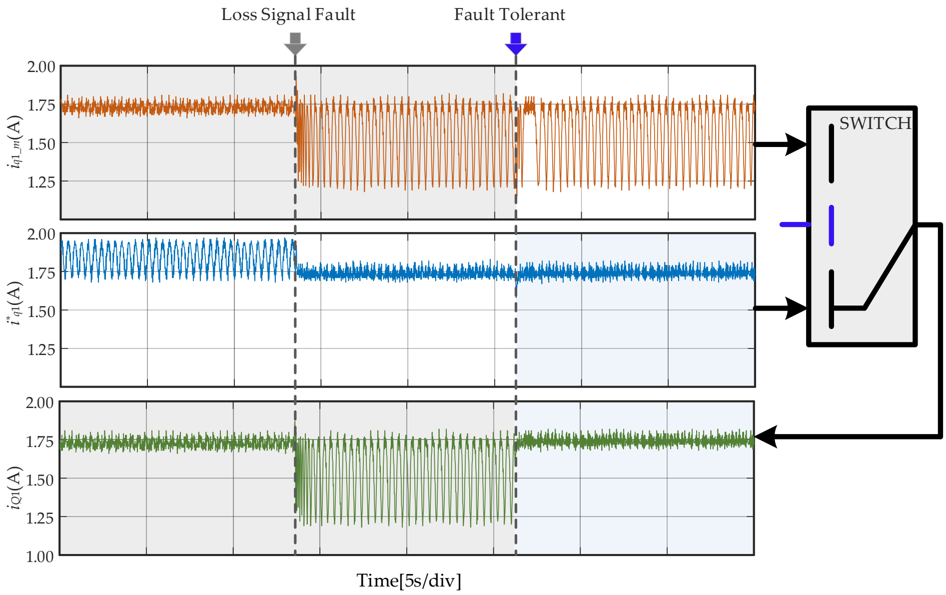

Figure 15. i_{q1_m}, i^*_{q1} and i_{Q1} in different conditions.

6.5. Gain Fault Tolerant

The proposed method can estimate the gain coefficient λ, which can be used as the correction factor of the fault phase current sensor, and can achieve fault-tolerant control directly and accurately.

In Figure 16a, when a 2.5 times gain fault of a phase-A_1 current sensor is set, the estimated coefficient λ has good tracking effect in normal and fault conditions. Therefore, fault-tolerant control can be realized by compensating the gain coefficient of the fault current sensor in DSP. After compensation, the estimated λ and i_{q1_m} are both restored to normal values.

Different from the existing algorithms, the proposed method can estimate the gain coefficient λ, which can be used as the correction factor of the fault sensor. The fault-tolerant control achieves tolerant accuracy by applying this factor.

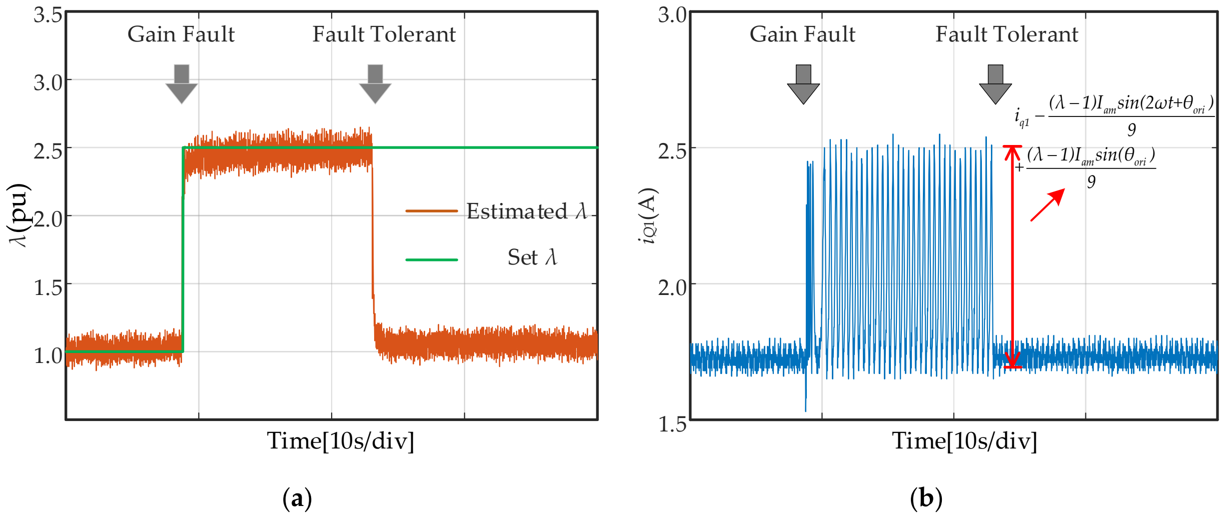

Figure 16. (**a**) Estimated λ and set λ; (**b**) i_{Q1}.

7. Conclusions

In this paper, a fault diagnosis and tolerant control method is proposed to different kinds of current sensor faults in multi-phase PMSM drives. It is desirable that the method utilizes the stator currents signal-processing, making it even simpler and less computationally demanding. It is also worth noting that the diagnosis variables have distinct characteristics which eliminate (to some extent) the margin of the design of the threshold. This method can distinguish between loss signal and gain faults effectively and lacks operating condition dependence. Moreover, the degree of current sensor gain fault can be quantitatively described by an estimated coefficient. Finally, fault diagnosis and tolerant control experiments are presented, which show the effectiveness and rapidity regarding the method. The optimization of diagnosis variables when multiple faults occur is the next focus.

Author Contributions: Conceptualization, X.Z. (Xudong Zhang); Funding acquisition, X.Z. (Xiaoqin Zheng); Methodology, X.Z. (Xudong Zhang); Software, X.L.; Visualization, X.L.; Writing—original draft, X.Z. (Xudong Zhang); Writing—review & editing, X.Z. (Xiaoqin Zheng). All authors have read and agreed to the published version of the manuscript.

Funding: This research was funded by the National Natural Science Foundation of China, grant number 51907093, 52037005, U2106217.

Institutional Review Board Statement: Not applicable.

Informed Consent Statement: Not applicable.

Data Availability Statement: Not applicable.

Acknowledgments: Thanks to Xinzhen Wu and Haifeng Wang for experimental guidance and writing suggestions for this article.

Conflicts of Interest: The authors declare no conflict of interest.

References

1. Liu, Z.; Fang, L.; Jiang, D.; Qu, R. A Machine-Learning-Based Fault Diagnosis Method with Adaptive Secondary Sampling for Multiphase Drive Systems. *IEEE Trans. Power Electron.* **2022**, *37*, 8767–8772. [CrossRef]
2. Chen, C.; Xu, J.; Yuan, X.; Wu, X. Characteristic Analysis of the Peak Braking Force and the Critical Speed of Eddy Current Braking in a High-Speed Maglev. *Energies* **2019**, *12*, 2622. [CrossRef]
3. Wang, H.; Zheng, X.; Yuan, X.; Wu, X. Low-Complexity Model-Predictive Control for a Nine-Phase Open-End Winding PMSM with Dead-Time Compensation. *IEEE Trans. Power Electron.* **2022**, *37*, 8895–8908. [CrossRef]
4. Wang, J.; Jiang, W.; Wang, S.; Lu, J.; Williams, B.W.; Wang, Q. A Novel Step Current Excitation Control Method to Reduce the Torque Ripple of Outer-Rotor Switched Reluctance Motors. *Energies* **2022**, *15*, 2852. [CrossRef]

5. Wang, H.; Wu, X.; Zheng, X.; Yuan, X. Virtual Voltage Vector Based Model Predictive Control for a Nine-Phase Open-End Winding PMSM With a Common DC Bus. *IEEE Trans. Ind. Electron.* **2022**, *69*, 5386–5397. [CrossRef]
6. Harikumaran, J.; Buticchi, G.; Galea, M.; Wheeler, P. Open Phase Fault Tolerant Control of Multi Three Phase Machines. *IEEE Trans. Power Electron.* **2021**, *2*, 535–544. [CrossRef]
7. Zhao, B.; Gong, J.; Tong, T.; Xu, Y.; Semail, E.; Nguyen, N.K.; Gillon, F. A Novel Five-Phase Fractional Slot Concentrated Winding with Low Space Harmonic Contents. *IEEE Trans. Magn.* **2021**, *57*, 1–5. [CrossRef]
8. Nguyen, N.K.; Meinguet, F.; Semail, E.; Kestelyn, X. Fault-Tolerant Operation of an Open-End Winding Five-Phase PMSM Drive With Short-Circuit Inverter Fault. *IEEE Trans. Ind. Electron.* **2016**, *63*, 595–605. [CrossRef]
9. Foo, G.H.B.; Zhang, X.; Vilathgamuwa, D.M. A Sensor Fault Detection and Isolation Method in Interior Permanent-Magnet Synchronous Motor Drives Based on an Extended Kalman Filter. *IEEE Trans. Ind. Electron.* **2013**, *60*, 3485–3495. [CrossRef]
10. Xiahou, K.S.; Lin, X.; Wu, Q.H. Current sensor fault-tolerant control of DFIGs using stator current regulators and Kalman filters. In Proceedings of the 2017 IEEE Power & Energy Society General Meeting (PESGM), Chicago, IL, USA, 16–20 July 2017; pp. 1–5.
11. Wang, G.; Hao, X.; Zhao, N.; Zhang, G.; Xu, D. Current Sensor Fault-Tolerant Control Strategy for Encoderless PMSM Drives Based on Single Sliding Mode Observer. *IEEE Trans. Transp. Electrific.* **2020**, *6*, 679–689. [CrossRef]
12. Yu, Y.; Zhao, Y.; Wang, B.; Huang, X.; Xu, D. Current Sensor Fault Diagnosis and Tolerant Control for VSI-Based Induction Motor Drives. *IEEE Trans. Power Electron.* **2018**, *33*, 4238–4248. [CrossRef]
13. Jlassi, I.; Estima, J.; El Khil, O.S.K.; Bellaaj, N.M.; Cardoso, A.J.M. A Robust Observer-Based Method for IGBTs and Current Sensors Fault Diagnosis in Voltage-Source Inverters of PMSM Drives. *IEEE Trans. Ind. Appl.* **2017**, *53*, 2894–2905. [CrossRef]
14. Zhang, G.; Zhou, H.; Wang, G.; Li, C.; Xu, D. Current Sensor Fault-Tolerant Control for Encoderless IPMSM Drives Based on Current Space Vector Error Reconstruction. *IEEE J. Emerg. Sel. Topics Power Electron.* **2020**, *8*, 3658–3668. [CrossRef]
15. Li, Z.; Wheeler, P.; Watson, A.; Costabeber, A.; Wang, B.; Ren, Y.; Bai, Z.; Ma, H. A Fast Diagnosis Method for Both IGBT Faults and Current Sensor Faults in Grid-Tied Three-Phase Inverters with Two Current Sensors. *IEEE Trans. Power Electron.* **2020**, *35*, 5267–5278. [CrossRef]
16. Venghi, L.E.; Aguilera, F.; de la Barrera, P.M.; De Angelo, C.H. Single-Observer Based Current Sensor Fault Tolerant Control for IM Traction Drives. *IEEE Lat. Am. Trans.* **2021**, *19*, 2087–2096. [CrossRef]
17. Sakthivel, R.; Kavikumar, R.; Mohammadzadeh, A.; Kwon, O.-M.; Kaviarasan, B. Fault Estimation for Mode-Dependent IT2 Fuzzy Systems With Quantized Output Signals. *IEEE Trans. Fuzz Syst.* **2021**, *29*, 298–309. [CrossRef]
18. Venghi, L.E.; Aguilera, F.; de la Barrera, P.M.; De Angelo, C.H. Detection and isolation of current-sensor and open-switch faults in electric traction drives. *IEEE Latin Am. Trans.* **2021**, *19*, 1335–1346. [CrossRef]
19. Ruba, M.; Nemeş, R.O.; Ciornei, S.M.; Marţiş, C. Simple and Robust Current Sensor Fault Detection and Compensation Method for 3-Phase Inverters. *IEEE Access* **2020**, *8*, 34820–34832. [CrossRef]
20. Wu, C.; Guo, C.; Xie, Z.; Ni, F.; Liu, H. A Signal-Based Fault Detection and Tolerance Control Method of Current Sensor for PMSM Drive. *IEEE Trans. Ind. Electron.* **2018**, *65*, 9646–9657. [CrossRef]
21. Huang, W.; Du, J.; Hua, W.; Lu, W.; Bi, K.; Zhu, Y.; Fan, Q. Current-Based Open-Circuit Fault Diagnosis for PMSM Drives With Model Predictive Control. *IEEE Trans. Power Electron.* **2021**, *36*, 10695–10704. [CrossRef]
22. Wang, W.; Tian, W.; Wang, Z.; Hua, W.; Cheng, M. A Fault Diagnosis Method for Current Sensors of Primary Permanent-Magnet Linear Motor Drives. *IEEE Trans. Power Electron.* **2020**, *36*, 2334–2345. [CrossRef]
23. Tran, C.D.; Palacky, P.; Kuchar, M.; Brandstetter, P.; Dinh, B.H. Current and Speed Sensor Fault Diagnosis Method Applied to Induction Motor Drive. *IEEE Access* **2021**, *9*, 38660–38672. [CrossRef]
24. Chakraborty, C.; Verma, V. Speed and Current Sensor Fault Detection and Isolation Technique for Induction Motor Drive Using Axes Transformation. *IEEE Trans. Ind. Electron.* **2015**, *62*, 1943–1954. [CrossRef]